Measurement of proton momentum distributions using a direct geometry instrument

2014 J. Phys.: Conf. Ser. 571 012007

(http://iopscience.iop.org/1742-6596/571/1/012007)

Journal of Physics: Conference Series **571** (2014) 012007 doi:10.1088/1742-6596/571/1/012007

Measurement of proton momentum distributions using a direct geometry instrument

R. Senesi[1,2], A. I. Kolesnikov[3], C. Andreani[1,2]

[1] Università degli Studi di Roma Tor Vegata, Dipartimento di Fisica and Centro NAST, via della Ricerca Scientifica 1, Rome 00133, Italy
[2] CNR-IPCF Sezione di Messina, Messina, Italy
[3]Chemical and Engineering Materials Division, Oak Ridge National Laboratory, Oak Ridge, Tennessee 37831, United States of America

E-mail: roberto.senesi@uniroma2.it

Abstract. We report the results of inelastic neutron scattering measurements on bulk water and ice using the direct geometry SEQUOIA chopper spectrometer at the Spallation Neutron Source (U. S. A.), with incident energy E_i= 6 eV. In this set up the measurements allow to access the Deep Inelastic Neutron Scattering regime. The scattering is centred at the proton recoil energy given by the impulse approximation, and the shape of the recoil peak conveys information on the proton momentum distribution in the system. The comparison with the performance of inverse geometry instruments, such as VESUVIO at the ISIS source (U. K.), shows that complementary information can be accessed by the use of direct and inverse geometry instruments. Analysis of the neutron Compton profiles shows that the proton kinetic energy in ice at 271 K is larger than in room temperature liquid water, in agreement with previous measurements on VESUVIO.

1. Introduction

Recent developments of the Deep Inelastic Neutron Scattering (DINS) technique for the measurement of atomic momentum distributions in materials provide an insight into the local environment of light (proton, deuteron, helium, lithium) and intermediate-weight (oxygen, fluorine, sodium, etc.) elements [1–10] in a variety of settings. The broader scope of these experiments is to directly measure the binding, anisotropy, and anharmonicity of the local potential experienced by the struck atoms. Isotropic quantum harmonic oscillator motion, although being the foundation for understanding diverse phenomena such as the vibrational modes of molecules, the motion of atoms in a lattice and the theory of heat capacity, is uncommon in materials such as metal hydrides and hydrogen-bonded systems, due to the presence of anisotropy and anharmonic effects. Indeed, the observation of atomic motion with nearly "perfect" quantum harmonic oscillations is regarded as an unexpected discovery, such as the recent Inelastic Neutron Scattering (INS) and DINS investigations of the quantum oscillations of nitrogen atoms in uranium nitride [11]. The most recent approaches involve the joint use of INS and DINS data to convey information on the anisotropy and anharmonic nature of light particle motions in condensed systems [3, 12–14]. The two techniques provide complementary information on the quantum nature of the motion on molecular systems such as water, which is characterised by proton motions reflecting the influence of internal stretching,

bending and external librational and translational modes; these are affected by different degrees of quantization and anharmonicities [15] and the measurements of both individual energy level differences and their zero-point values allows to determine the extent of nuclear quantum effects in the system. Indeed on one hand DINS measures almost directly the momentum distribution, $n(p)$, and kinetic energy, $\langle E_K \rangle$, of the equilibrium state, that means the kinetic energy of ground and excited states for the low energy vibrations (comparable with k_BT) and, at room temperatures and below, only the ground state for the intramolecular bending and stretching modes of water molecule (because at T$\sim$300 K these modes are not excited at all). On the other hand INS in energy loss configuration measures the transition from the ground state to the first excited state, and the data are often interpreted in the frame of harmonic normal mode analysis, deriving the hydrogen-projected density of states, $g(E)_H$. The latter quantity can be used to obtain an independent estimate of the mean kinetic energy $\langle E_K \rangle$.

In cases where the system is anharmonic the values of kinetic energies derived from INS will be in general different compared to the values from DINS experiments, even at low temperatures [14]. This finding is in line with recent theoretical quantum Monte Carlo simulation studies of momentum distribution and vibrational dynamics in ice, where it was shown that the analysis of proton displacements in the harmonic assumption leads proton kinetic energy values 10% larger than those obtained directly from the Path Integral Car-Parrinello Molecular Dynamics simulation [16].

Within this framework it appears that the development of instrumentation with the capability to operate as DINS, as well as INS, spectrometers will provide a step forward in the elucidation of nuclear quantum effects [11], besides expanding the available kinematic ranges for other classes of investigations, such as the probing of electronic structures of correlated electron systems [17]. This approach has been proposed previously [18], and can be regarded as part of the long history of experiments with eV neutrons in neutron physics [19, 20]. In 1984 Brugger and co-workers [21] reported calculations and experimental tests of a prototype time of flight spectrometer for inelastic scattering using eV neutrons operating in both direct and inverse geometries. The spectrometer made use of resonant filters in the eV range to define the incident (direct geometry) or scattered (inverse geometry) neutron energies. It was reported that both geometry configurations showed energy resolutions of the same order of magnitude if the neutron flight paths are optimised. Differences in the kinematics cuts in the wave vector and energy transfers space showed that the obvious advantage of the inverse geometry is that there is no upper bound to the energy transfers which may be achieved; whereas in the direct geometry method, energy transfers are bounded by the incident energy [21]. The research programme on DINS studies for condensed matter has been mainly carried out at the ISIS facility on the eVS, then VESUVIO, spectrometer [22, 23], with early developments at the Argonne and Los Alamos National Laboratories [24, 25] and at the KENS source in Japan [26], along with more recent developments at the Bariloche neutron source (AR) [27]. All of the above instruments were built in the inverse geometry configuration, thanks to the more extended kinematic range available and for the superior energy resolution around the recoil excitation energies, as compared to direct geometry [23]. Interest in the potential of direct geometry instruments has been recently revised to extend the incident energy range up to 150 eV for the study of proton scattering cross sections [28], and, in the 3 eV range, for the probing of electronic excitations [17].

In this work we have used the SEQUOIA Fine-Resolution Fermi Chopper Spectrometer at the Spallation Neutron Source, Oak Ridge National Laboratory (U. S. A.), to carry out DINS measurements on samples of bulk water and ice at 271 K and 293 K, respectively, using incident neutrons of energy up to 6 eV. Section 2 describes the experiment and in Section 3 we discuss the data analysis and results. Section 4 reports the conclusions.

2. Experiment

The DINS experiment was carried out on ice and liquid water at 271 K and 293 K, respectively, using SEQUOIA [29]. An high neutron incident energy, E_i= 6000 meV, was chosen in order to simultaneously access high wave vectors ($q \gtrsim 20$ Å^{-1}) and energy ($\hbar\omega \gtrsim 1000$ meV) transfers. The sample container was a flat aluminum holder, with 50 x 50 mm^2 cross-section and internal thickness 0.25 mm, with Teflon coated inner surface. The container was located perpendicular to the incident neutron beam. Data for the T= 293 K sample were recorded for approximately 3 hours, corresponding to 1.2 $\times 10^{13}$pC of proton charge collected on the spallation target, and for the T=271 K for approximately 1.5 hours, corresponding to 0.6 $\times 10^{13}$pC of proton charge collected on the spallation target. The measurements were performed for a sample in the container, the empty container, the background and a vanadium plate of the same sample geometry. Neutron counting was carried out using ^{3}He neutron detectors, covering a scattering angular range 4° $<2\theta <$ 56°, with an angular increment of 0.26°. The background from the empty container was subtracted from the raw data counts, and the vanadium run provided data for detector calibration and intensity normalization of the spectra. The data treatment also included the corrections for efficiency of detectors as a function of energy and for the kinematical factor k_f/k_i.

3. Results and discussion

In Figure 1 the intensity map of the spectrum of ice obtained with nominal incident energy of E_i= 5617 meV is plotted. The horizontal axis is wave vector transfer and the vertical axis is energy transfer. We have superimposed three lines representing the expected proton recoil excitation with a recoil width equal to $\sigma_H = 5$Å^{-1}, corresponding to $\hbar\omega_R = \hbar^2q^2/(2M)$, $\hbar\omega = [\hbar^2q^2/(2M) \pm \hbar^2q\sigma_H/M]$, respectively, where M is the proton mass . One can clearly identify that the inelastic scattering intensity is centred at the proton recoil excitation line. The intensity at high wave vector and low energy values originates from the zero-energy transfer elastic contribution which is broadened and dominated by the instrumental resolution, and by the oxygen recoil excitation line. It is not possible to separate these two contribution for the present value of E_i.

The intensity at the energy transfers well above the proton recoil width is due to a background from fast delayed neutrons partially overlapping with neutrons selected with Fermi chopper. This contribution is independent of the scattering angle and is shown in Figure 2 for the ice sample. In this figure the fixed angle scattering intensities are reported for a series of scattering angles between 4 degrees and 56 degrees, and show that the background is the same at all scattering angles and is non negligible for energy transfers above 4500 meV. This finding is confirmed by inspection of the time of flight spectrum recorded by the SEQUOIA incident neutron monitor, Monitor 1; the spectrum reported in Figure 3 is acquired by a phasing and opening of the background T0 chopper just before the requested E_i=5617 meV, and it is shown that neutrons selected with the Fermi chopper with energy 5617 meV are superimposed on the tail of fast delayed neutrons.

We found that the background on the fixed angle spectra can be modeled by a fifth-order polynomial.

The analysis of DINS data is carried out within the framework of the Impulse Approximation (IA) [22], where the incident neutron wavelengths are much smaller than the inter-atomic spacing and thus atoms scatter incoherently, with scattered intensity being the sum of intensities from individual atoms in the sample, with conservation of the total kinetic energy and momentum of the neutron and the atom. In the IA regime the inelastic neutron scattering cross section is related in a simple way to the atomic momentum distribution, $n(\mathbf{p})$. The neutron scattering

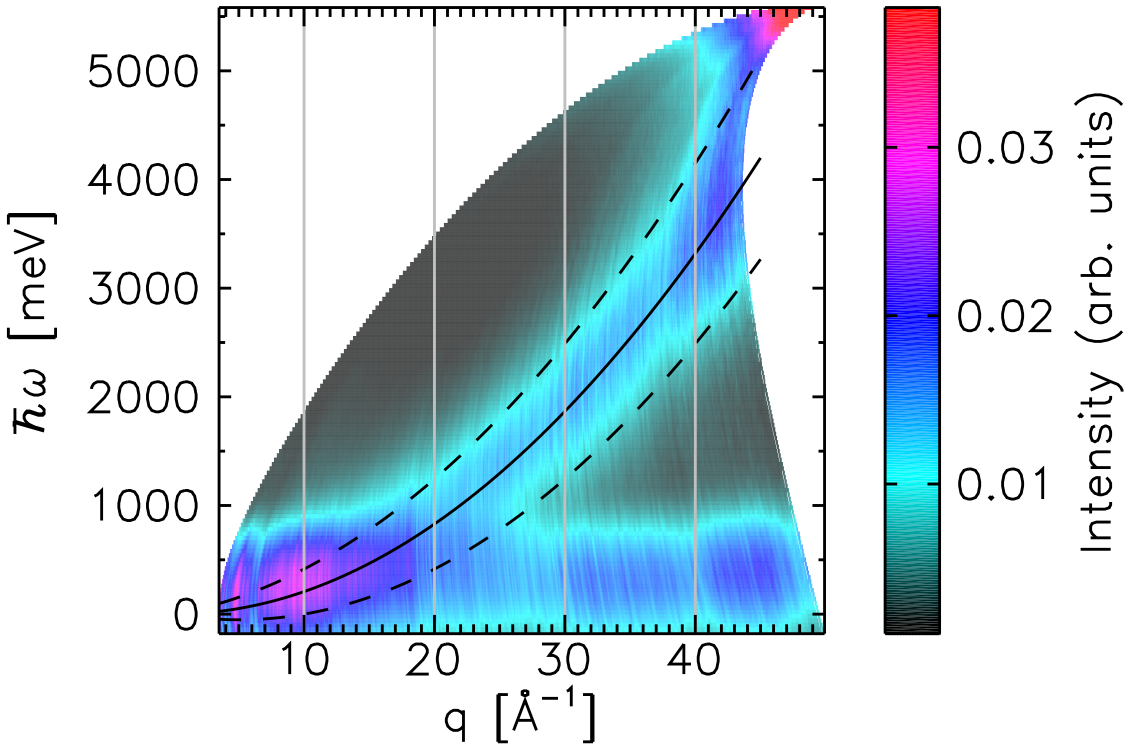

Figure 1. (Color online) Scattering intensity map of energy-wave vector space obtained on SEQUOIA using incident neutrons of 6000 meV (effective energy of 5617 meV) at T=271K. The theoretical proton recoil excitation lines with a width of 5 Å^{-1} are reported as continuous and dashed black lines.

function $S_{\text{IA}}(\mathbf{q},\omega)$ is:

$$S_{\text{IA}}(\mathbf{q},\omega) = \int \mathbf{n}(\mathbf{p})\, \delta\left(\omega - \omega_{\mathbf{R}} - \frac{\mathbf{p}\cdot\hat{\mathbf{q}}}{\mathbf{M}}\right) \mathrm{d}\mathbf{p} \tag{1}$$

$$\frac{\hbar q}{M} S_{\text{IA}}(\mathbf{q},\omega) = J_{\text{IA}}(y,\hat{\mathbf{q}}) = \int n(\mathbf{p}) \delta\left(y - \mathbf{p}\cdot\hat{\mathbf{q}}\right) \mathrm{d}\mathbf{p} \tag{2}$$

where $(\mathbf{q},\omega)$ are the wave vector and energy transfers, M is the mass of the struck atom , $y = \frac{M}{\hbar q}\left[\omega - \frac{\hbar q^2}{2M}\right]$ is the particle momentum along the $\hat{\mathbf{q}}$ direction, and $J_{\text{IA}}(y,\hat{\mathbf{q}})$ is the neutron Compton Profile (NCP) [22]. [1] The above equations assume that the measurements are carried out at constant wave vector transfer and varying only the energy. In practice, the width and intensity of the scattering signal depend on the trajectory in the $\hbar\omega, q$ plane of the measurement (see Fig. 1). The trajectories are different in the case of inverse and direct geometry [23,28,30]. In particular, on VESUVIO, the single detector trajectories intersect the proton recoil line more tangentially [23] than on SEQUOIA. As shown in Equation 2, the width of the scattering arises from the width of the proton recoil line shape (see Fig. 1), which is dependent on the width of the proton momentum distribution in the system. Indeed, a reliable DINS experiment should include the measurement of the full recoil line shape, *i.e.* extending for at least four standard

[1] For consistency with previous literature and ease of notation we write the momentum as a wave vector.

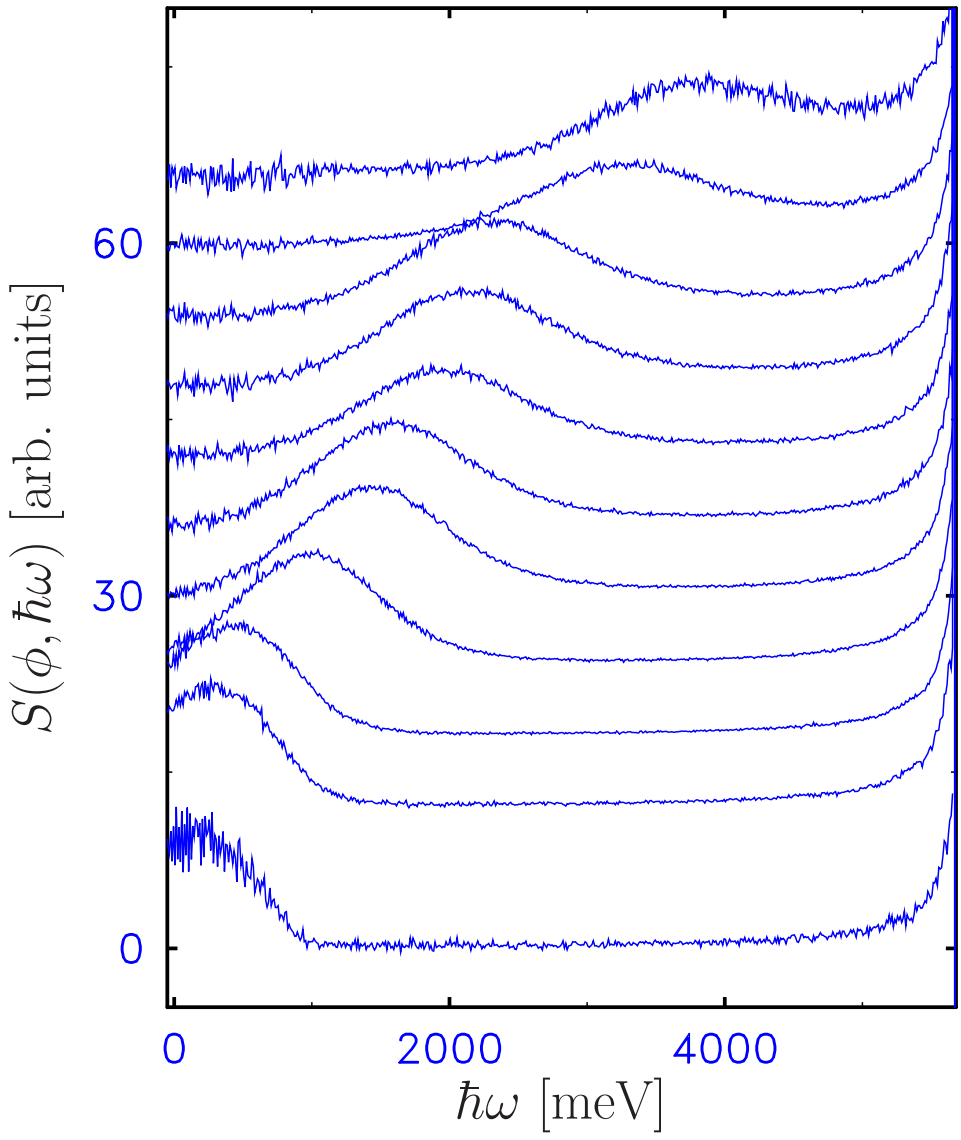

Figure 2. (Color online) Fixed angle scattering intensities for a selection of scattering angles between 4 degrees and 56 degrees; these were obtained using standard routines available on the instrument, and are shifted upwards for clarity.

deviations from the centroid of the recoil peak [31]. Typically, the standard deviations of the proton recoil peaks are of the order of $\hbar^2 q\sigma_H/M$, where σ_H, being of the order of 5 Å^{-1}, is the standard deviation of the momentum distribution, $n(\mathbf{p})$. Figure 4 reports an example of

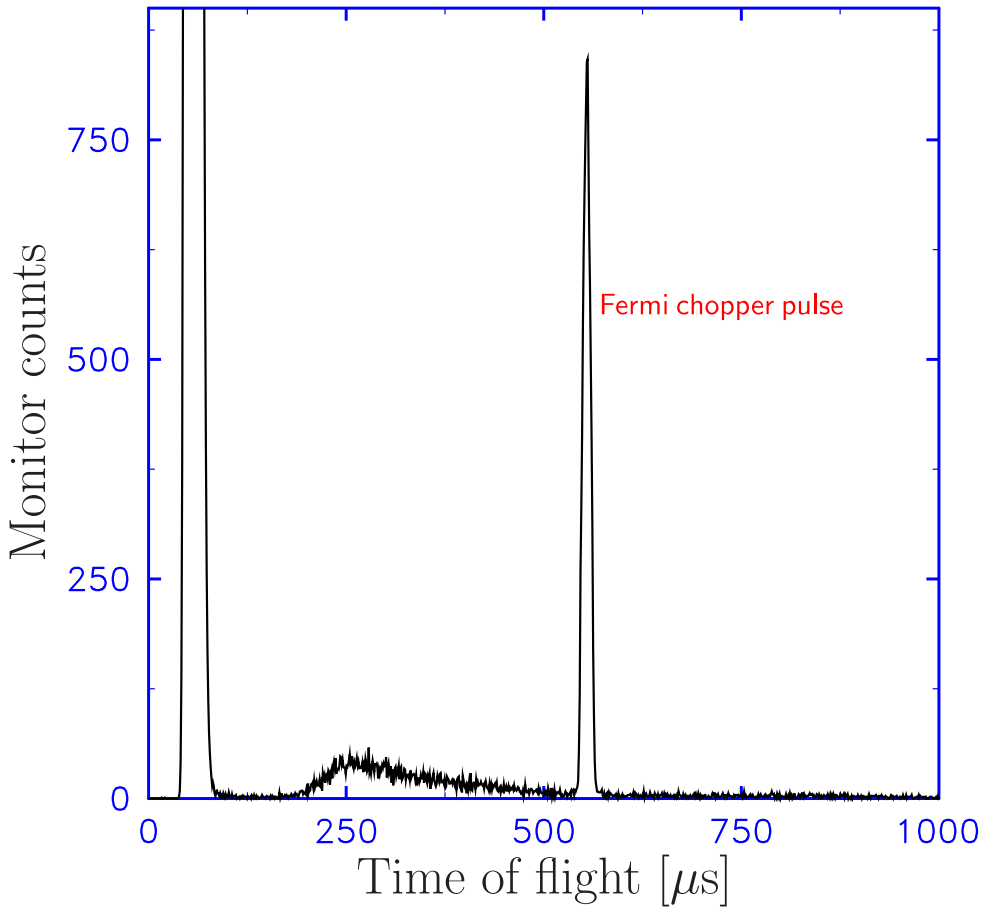

Figure 3. (Color online) Example of time of flight intensity recorded by the incident Monitor 1, placed at 18.23 m from the moderator. The pulse from the Fermi chopper is centred at approximately 550 μs . The peak at approximately 250 μs is a consequence of monitor dead-time after saturation of the monitor itself at short time, due to very large neutron flux (of high energy neutrons), and transmission of the delayed fast neutrons through both the background T0 and Fermi choppers.

the crossings of the detector trajectories and the proton recoil at different widths of the recoil line shape. The central recoil line marks the energy and wave vector positions of the centroid of the scattered intensity, which is crossed once for each detector trajectory. The recoil lines corresponding to a broadening of one standard deviation (red dot-dashed lines) cross the detector trajectories twice, therefore a fixed angle scan samples the same proton momentum value two times (red crosses in Fig. 4). The same behaviour is found for two and three(blue short-dashed lines) -standard deviations broadening.

Indeed the measured value of proton momentum, y, depends on the distance between the

detector trajectory and the recoil trajectory, that is on the difference $\frac{M}{\hbar q}\left[\omega - \frac{\hbar q^2}{2M}\right]$, which is non-monotonic (see Fig. 4) and causing double counting of the scattering intensity for $y \geq 5\text{Å}^{-1}$.

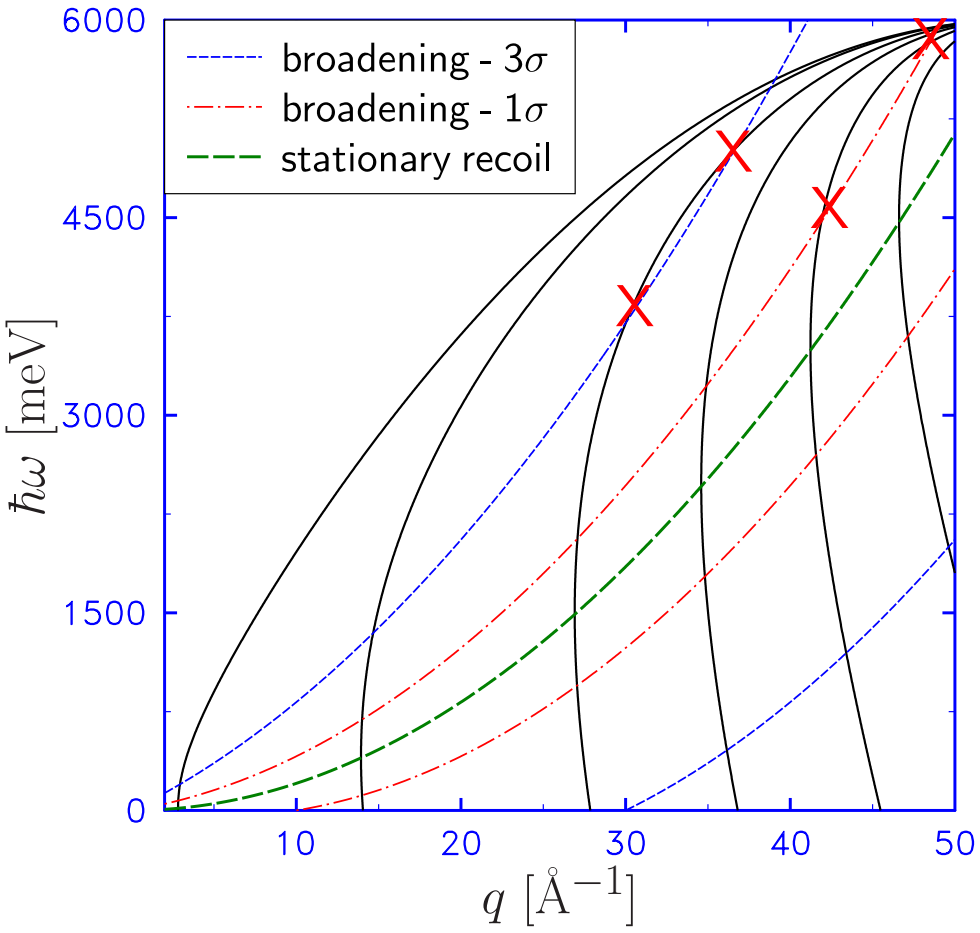

Figure 4. (Color online) Crossing of detector trajectories (black continuous lines), for representative scattering angles between 4 degrees and 60 degrees, with the proton recoil line (green dashed line). The red dot-dashed lines and blue short-dashed lines represent the broadening of the recoil due to finite momentum width corresponding to one (red dot-dashed lines) and three (blue short-dashed lines) standard deviations. The X signs are examples of the intersections between the detector trajectories and the momentum-broadened proton recoil.

This means that a line shape analysis of the spectra measured at constant scattering angle cannot provide a direct information on the shape and intensity of $S_{\text{IA}}(\mathbf{q},\omega)$, due to the double counting of the same proton momentum at different $\hbar\omega, q$ values. It has been proposed that the use of a Waller-Froman Jacobian relating the free recoil excitation and the wave vector transfer as a function of the scattering angle can be employed to relate a constant-angle scan

to a constant-q scan [28]. Indeed the above Jacobian is calculated assuming $\hbar\omega \equiv \hbar^2 q^2/(2M)$, that is, a non-physical situation in which all proton atoms have zero momentum, which is never realised in nature. The resulting Jacobian-transformed spectra would contain an overestimation of the high proton momentum tail of $S_{\rm IA}(\mathbf{q},\omega)$ [28]. Based on the above findings we conclude that DINS measurements on direct geometry instruments cannot be reliably analysed using constant scattering angle spectra. On the other hand, constant-q slices allow to correctly analyse the DINS spectra.

Data for ice, water, and the corresponding empty container signals, have then been transformed into constant-q slices for three q values, namely $q = 30 \pm 1$ Å^{-1}, $q = 34 \pm 1$ Å^{-1}, $q = 40 \pm 1$ Å^{-1}. These values allow to obtain recoil spectra extending to proton momentum values $\mathbf{p}\cdot\hat{\mathbf{q}} \simeq \pm\ 20$ Å^{-1}. In this respect there are specific advantages and disadvantages of direct geometry compared to inverse geometry DINS measurements for the proton: the advantage is that in principle the fine detector coverage and the kinematic plane of the direct geometry allow an extended choice of q slices; the disadvantage is that the $\mathbf{p}\cdot\hat{\mathbf{q}}$ range accessed is $\simeq 35$ % smaller than on VESUVIO ($\mathbf{p}\cdot\hat{\mathbf{q}} \simeq \pm\ 20$ Å^{-1} compared to $\mathbf{p}\cdot\hat{\mathbf{q}} \simeq \pm\ 30$ Å^{-1} for inverse geometry) because of the kinematic constraints (see , Fig.1 and Fig.4), and this limits the choice of suitable constant-q slices at high wave vector transfers, as shown in Fig.4 . The three spectra for the ice sample measurement are reported in Figure 5. The figure shows the shift of the recoil centroids to higher energy transfers at increasing values of wave vector transfer, as expected from the Impulse Approximation prediction. The high energy transfers tail shows the contribution due to background signals from fast neutrons as discussed above (see Fig. 2) . The spectra have been transformed in momentum space, rebinned to constant bin width of 0.5 Å^{-1} and normalised, yielding the neutron Compton profiles for the samples investigated. It has to be stressed that Equation 2 is assumed to be strictly valid in the limit of infinite wave vector transfer. From the experimental point of view, the deviations from the asymptotic regime, the broadening due to the instrumental resolution, and the isotropic nature of the sample, are accounted for by the following representation of the NCP [22]:

$$F(y,q) = [J_{\rm IA}(y) + \Delta J(y,q)] \otimes R(y,q). \tag{3}$$

where $\Delta J(y,q)$ accounts for the finite-q correction terms (final state effects) [32], $R(y,q)$ is the instrumental resolution function and for an isotropic sample the particle momentum distribution is spherically averaged and depends only on the modulus of $\mathbf{p}$, therefore $J_{\rm IA}(y) = 2\pi \int_{|y|}^{\infty} p\, n(p)\, dp$ [22].

Figure 6 reports the three experimental NCP for the ice and water samples, respectively. The plots show the raw differences, $[F(y,q)_{ice} - F(y,q)_{water}]$, between ice and water ; these are directly related to the differences of proton momentum distributions in the two samples. The differences are small, but it can be noticed that $F(y,q)_{ice}$ has a slightly lower height at the peak centre and larger wings in the ranges -10 Å$^{-1} \leq y \leq -5$ Å^{-1}, 5 Å$^{-1} \leq y \leq 10$ Å^{-1}. This is indeed shown by the differences which are positive, on average, in the above ranges, and negative around the peak centre. Such a behaviour suggests that the neutron Compton profile, and thus the proton momentum distribution, in ice at 271 K is broader than liquid water at room temperature. Figure 7 reports a comparison between the $F(y,q)$ for ice for $q = 34 \pm 1$ Å^{-1} from the present experiment and the corresponding angle averaged- NCP, $\bar{F}(y)$, from a previous VESUVIO measurement on the same sample at the same temperature, T=271 K [2]. It can be noticed that the shapes are similar, with the exception of a reduced momentum range for the SEQUOIA measurement and the presence of the above mentioned background.

In order to analyse the line shapes of the NCP for the present measurements, the data have been fitted using the ice NCP as a reference: the model line shape for $F(y,q)$ at the three q values is a Compton profile of the form $[J_{\rm IA}(y) + \Delta J(y,q)]$ with parameters fixed to the values from ref. [2], broadened by the resolution function, $R(y,q)$; the latter is assumed to be a

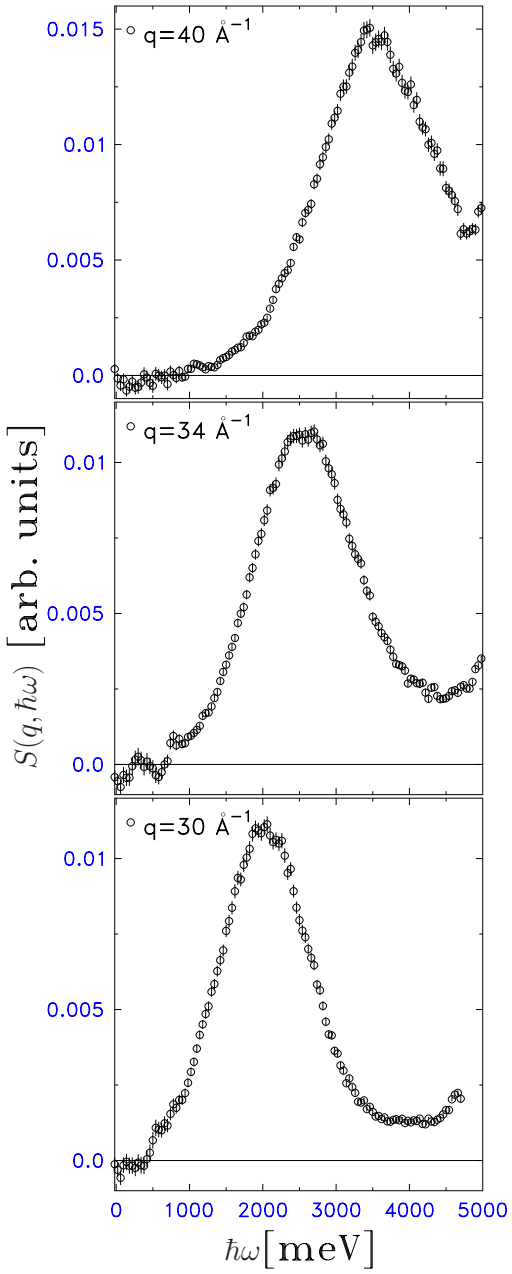

Figure 5. (Color online) Proton recoil spectra for the ice sample at $q = 30 \pm 1$ Å^{-1} (lower panel), $q = 34 \pm 1$ Å^{-1} (middle panel), $q = 40 \pm 1$ Å^{-1} (top panel)

Gaussian with the standard deviation as a free parameter, plus a parabolic function to model the background at high momenta. The final state effects term, $\Delta J(y, q)$, is expected to be smaller on VESUVIO data than on SEQUOIA, since its magnitude is proportional to inverse powers of q, being the q-range on VESUVIO extended to values one order of magnitude larger than on SEQUOIA [33]. However, preliminary tests on the sensitivity of the line shape modeling showed that, for the present data, the contribution of final state effects terms of order $1/q^2$ and beyond were negligible. The model function was fitted to the data using a nonlinear minimization

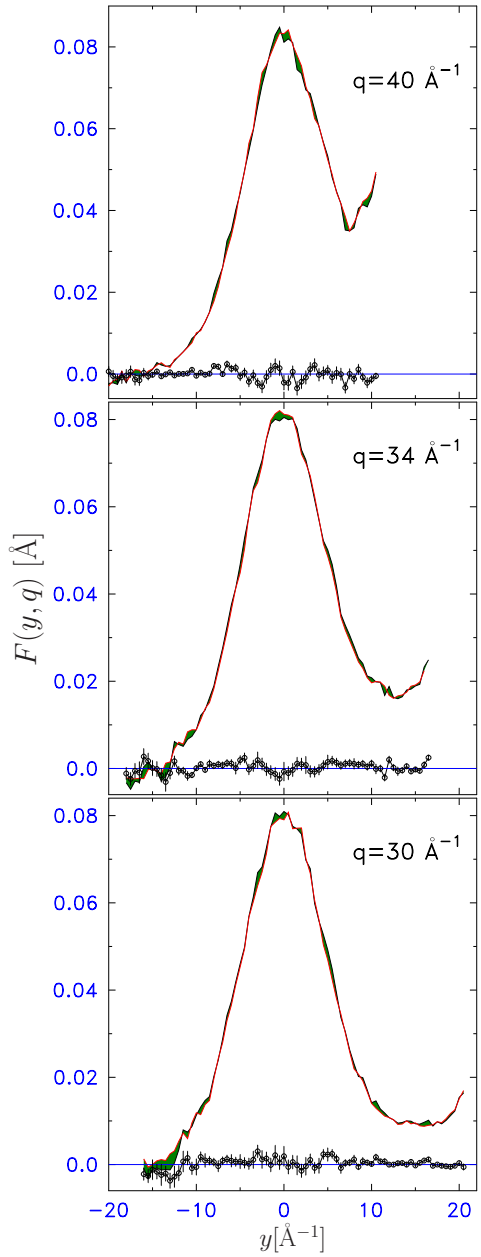

Figure 6. (Color online) Proton neutron Compton profiles for the ice (black lines) and water (red lines) samples at $q = 30 \pm 1$ Å^{-1} (lower panel), $q = 34 \pm 1$ Å^{-1} (middle panel), $q = 40 \pm 1$ Å^{-1} (top panel). The green filling between the profiles at each q value highlights the differences between ice and water. The panels also report the raw differences, $[F(y,q)_{ice} - F(y,q)_{water}]$ as black dots with error bars, which oscillate around zero.

routine described in ref. [2]. The fitting provided the three sets of parameters describing the resolutions and background shapes at the three q values.

Subsequently, the fitting procedure has been applied to the water data by fixing the resolution and background parameters to the values found for ice, while the width (standard deviation)

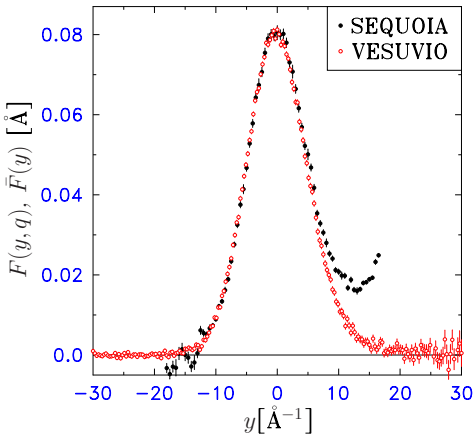

Figure 7. (Color online) Proton neutron Compton profiles for ice (solid black circles with error bars) from the present measurement, and the corresponding angle averaged- NCP, $\bar{F}(y)$, from a previous VESUVIO measurement on the same sample at the same temperature, T=271 K (red open circles) [2].

of $J_{\rm IA}(y)$ for water is a free fitting parameter. The results of the analysis of the water data provided an estimate of the standard deviation of the proton momentum distribution in water, averaged over the three q values, namely: $\sigma_{water} = (4.91 \pm 0.03)$ Å^{-1}. This value corresponds to a proton kinetic energy, $\langle E_K \rangle_{water} = \frac{3\hbar^2}{2M}\,\sigma^2_{water} = 151 \pm 2$ meV. This has to be compared with the proton kinetic energy in ice at T=271 K, namely 156 ± 2 meV from ref. [2]. This finding confirms qualitatively previous comparisons of the experimental determinations of proton kinetic energy in ice close to the triple point and liquid water at room temperature [34]. Theoretical works on the determination of proton kinetic energies in water relate the decrease in hydrogen bonding in the liquid, and the more flexible environment, to be associated to either a negligible difference between the kinetic energies in the solid and the liquid, or to a nearly continuous behavior [12]. The present result suggest on the other hand an unexpected decrease of in the liquid phase, which should be investigated with higher accuracy measurements and calculations. Interestingly, the deuterium kinetic energy in heavy water does not show such a behavior, being the kinetic energy in the solid close to the triple point slightly lower than in the room temperature liquid, in agreement with theory [3]. The present results suggests that the different degrees of anharmonicity and hydrogen bonding in light water compared to heavy water are at the origin of these quantum differences in the local environment of the proton in the solid and liquid phases.

4. Conclusions

The measurements presented here allowed an assessment of the performance of SEQUOIA for DINS measurements of proton momentum distribution. The data analysis confirmed qualitatively that the kinetic energy in room temperature water is lower than in ice close to the triple point, in line with previous VESUVIO measurements. It is suggested that this property is ascribed to the competition between hydrogen bonding and anharmonicity in the two phases, with different influence of quantum effects with respect to heavy water. From the instrumental point of view, the complementarity between direct and inverse-types of instrument can convey information on specific advantages and disadvantages of chopper spectrometer with respect to inverse geometry spectrometers, namely: 1) Count rate and flexibility; at present SEQUOIA

has a factor of $\simeq 8$ larger counting capabilities over VESUVIO for this type of measurements. This is mostly due to the higher neutron source flux with respect to ISIS. The flexibility allows to operate with a large number of incident energies, while on VESUVIO this choice is limited to one final energy value. 2) Detector solid angle coverage; this allows to operate constant-q slices for data analysis with a larger flexibility compared to VESUVIO [33]. 3) Kinematic trajectories; these are limited with respect to VESUVIO and do not allow for a complete scan of the full proton momentum range, with a reduction of $\simeq 35$ % with respect to VESUVIO. The kinematic trajectories do not allow to analyse constant-angle spectra. More optimised data sets in this respect may be obtained for studies on deuteron containing samples [35]. Measurements on even heavier masses would however lack the mass-specific separation capability [36, 37]that can be achieved on VESUVIO [9]. 4) Fast neutrons background and resolution; the optimised phasing in the current set up does not allow to completely suppress the background, preventing fine line shape analysis beyond the determination of the standard deviation. Such optimisation should require the use of sequential choppers. The proton momentum space resolution is presently worse than on VESUVIO [23, 38], limiting the line shape analysis capability.

The above considerations show that direct geometry instruments can be used for large energy transfers to provide complementary information to inverse geometry instruments, with a series of limitations that still do not allow to reach the capabilities of inverse geometry configuration. Substantial improvements on the instrumental resolution can be achieved with new chopper design to optimise slits curvature and distances. These optimisation strategies would be however most effective in the case of deuteron studies rather than for proton ones.

5. Acknowledgments

This work was supported within the with the support of META (Materials Enhancement for Technological Applications) PIRSES-GA-2010-269182, Marie Curie Actions, People, VII Framework Programme, and within the CNR-STFC Agreement No. 06/20018 concerning collaboration in scientific research at the spallation neutron source ISIS. The neutron scattering experiment at Oak Ridge National Laboratorys Spallation Neutron Source was sponsored by the Scientific User Facilities Division, Office of Basic Energy Sciences, US Department of Energy.

References

[1] Reiter G F, Senesi R and Mayers J 2010 *Physical Review Letters* **105** 148101 (*Preprint* 1002.4398)
[2] Flammini D, Pietropaolo A, Senesi R, Andreani C, McBride F, Hodgson A, Adams M A, Lin L and Car R 2012 *The Journal of Chemical Physics* **136** 024504
[3] Romanelli G, Ceriotti M, Manolopoulos D E, Pantalei C, Senesi R and Andreani C 2013 *The Journal of Physical Chemistry Letters* **4** 3251–3256 (*Preprint* http://pubs.acs.org/doi/pdf/10.1021/jz401538r) URL http://pubs.acs.org/doi/abs/10.1021/jz401538r
[4] Krzystyniak M and Fernandez-Alonso F 2011 *Physical Review B - Condensed Matter and Materials Physics* **83** 134305
[5] Krzystyniak M and Abdul-Redah T 2010 *Physical Review B - Condensed Matter and Materials Physics* **82** 064301
[6] Krzystyniak M 2010 *Journal of Chemical Physics* **133** 144505
[7] Krzystyniak M, Adams M A, Lovell A, Skipper N T, Bennington S M, Mayers J and Fernandez-Alonso F 2011 *Faraday Discuss.* **151**(0) 171–197 URL http://dx.doi.org/10.1039/C1FD00036E
[8] Seel A G, Ceriotti M, Edwards P P and Mayers J 2012 *Journal of Physics Condensed Matter* **24** J5401
[9] Krzystyniak M, Richards S, Seel A and Fernandez-Alonso F 2013 *Physical Review B - Condensed Matter and Materials Physics* **88** 184304
[10] Price D and Fernandez-Alonso F 2013 *Experimental Methods in the Physical Sciences* **44** 1–136
[11] Aczel A A, Granroth G E, MacDougall G J, Buyers W J L, Abernathy D L, Samolyuk G D, Stocks G M and Nagler S E 2012 *Nature Communications* **3** 1124 (*Preprint* 1206.3597)
[12] Finkelstein Y and Moreh R 2014 *Chemical Physics* **431** 58–63
[13] Andreani C, Romanelli G and Senesi R 2013 *Chemical Physics* **427** 106–110

[14] Senesi R, Flammini D, Kolesnikov A I, Murray É D, Galli G and Andreani C 2013 *Journal of Chemical Physics* **139** 074504
[15] Marechal Y 2006 *The Hydrogen Bond and the Water Molecule: The Physics and Chemistry of Water, Aqueous and Bio-Media* (Elsevier Science) ISBN 9780080469294
[16] Lin L, Morrone J A, Car R and Parrinello M 2011 *Physical Review B* **83** 220302
[17] Kim Y J, Sorini A P, Stock C, Perring T G, van den Brink J and Devereaux T P 2011 *Physical Review B* **84**(8) 085132 URL `http://link.aps.org/doi/10.1103/PhysRevB.84.085132`
[18] Silver R N 1984 *Workshop held in Los Alamos, N. Mex., 13-15 Feb. 1984* pp 345–648
[19] Lamb W E 1939 *Physical Review* **55** 190–197
[20] Gol'danskii V I 1957 *Soviet Phys. JETP* **4** 604
[21] Brugger R M, Taylor A D, Olsen C E, Goldstone J A and Soper A K 1984 *Nuclear Instruments and Methods in Physics Research* **221** 393 – 407 ISSN 0167-5087 URL `http://www.sciencedirect.com/science/article/B73DP-478HFR2-20/2/c56fd981fa54c58efa2c6d5177da312c`
[22] Andreani C, Colognesi D, Mayers J, Reiter G F and Senesi R 2005 *Advances in Physics* **54** 377
[23] Pietropaolo A and Senesi R 2011 *Physics Reports* **508** 45–90
[24] Crawford R K 1986 *Proceedings of the Ninth International Collaboration on Advanced Neutron Sources* pp 397–430
[25] Taylor A, Robinson R A and Seeger P A 1984 *Nuclear Instruments and Methods in Physics Research* **224** 133–141
[26] Carpenter J and Watanabe N 1983 *Nuclear Instruments and Methods in Physics Research* **213** 311 – 316 ISSN 0167-5087
[27] Rodríguez Palomino L A, Blostein J J and Dawidowski J 2011 *Nuclear Instruments and Methods in Physics Research A* **646** 142–152
[28] Stock C, Cowley R A, Taylor J W and Bennington S M 2010 *Physical Review B* **81** 024303 (*Preprint* `0907.1945`)
[29] Granroth G E, Kolesnikov A I, Sherline T E, Clancy J P, Ross K A, Ruff J P C, Gaulin B D and Nagler S E 2010 *Journal of Physics: Conference Series* **251** 012058
[30] Brugger R 1984 *Nuclear Instruments and Methods in Physics Research* **221** 393–407
[31] Senesi R 2012 *Nuclear Instruments and Methods in Physics Research A* **661** 70–76
[32] Sears V F 1984 *Phys. Rev. B* **30** 44–51
[33] Senesi R, Pietropaolo A and Andreani C 2008 *Nuclear Instruments and Methods in Physics Research A* **594** 244–252
[34] Senesi R, Romanelli G, Adams M and Andreani C 2013 *Chemical Physics* **427** 111–116
[35] Diallo S O private communication
[36] Seel A, Krzystyniak M and Fernandez-Alonso F *Journal of Physics: Conference Series* This issue
[37] Krzystyniak M, Seel A, Richards S, Gutmann M J and Fernandez-Alonso F *Journal of Physics: Conference Series* This issue
[38] Mayers J, Gidopoulos N I, Adams M A, Reiter G, Andreani C and Senesi R 2011 *Phys. Rev. B* **84**(5) 056301